ACS SyntheticBiology

Research Article

pubs.acs.org/synthbio

# Refactoring and Optimization of Light-Switchable *Escherichia coli* Two-Component Systems

Sebastian R. Schmidl,[†] Ravi U. Sheth,[†] Andrew Wu,[†] and Jeffrey J. Tabor*[,†,‡]

[†]Department of Bioengineering and [‡]Department of Biochemistry and Cell Biology, Rice University, 6100 Main Street, Houston, Texas 77005, United States

Supporting Information

**ABSTRACT:** Light-switchable proteins enable unparalleled control of molecular biological processes in live organisms. Previously, we have engineered red/far-red and green/red photoreversible two-component signal transduction systems (TCSs) with transcriptional outputs in *E. coli* and used them to characterize and control synthetic gene circuits with exceptional quantitative, temporal, and spatial precision. However, the broad utility of these light sensors is limited by bulky DNA encoding, incompatibility with commonly used ligand-responsive transcription factors, leaky output in deactivating light, and less than 10-fold dynamic range. Here, we compress the four genes required for each TCS onto two streamlined plasmids and replace all chemically inducible and evolved promoters with constitutive, engineered versions. Additionally, we systematically optimize the expression of each sensor histidine kinase and response regulator, and redesign both pathway output promoters, resulting in low leakiness and 72- and 117-fold dynamic range, respectively. These second-generation light sensors can be used to program the expression of more genes over a wider range and can be more easily combined with additional plasmids or moved to different host strains. This work demonstrates that bacterial TCSs can be optimized to function as high-performance sensors for scientific and engineering applications.

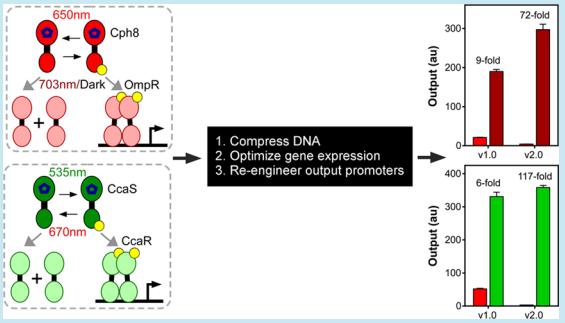


**KEYWORDS:** *optogenetics, Escherichia coli, two component system, phytochrome, cyanobacteriochrome, refactoring*

Systems-level biological processes such as metabolism, cellular differentiation, and multicellular development require precisely coordinated analog, temporal, and spatial gene expression patterns.[1−4] Therefore, to study and engineer biological systems, technologies for programming gene expression quantitatively, and in space and time, are needed.[5,6] Typically, researchers control gene expression using small-molecule chemical effectors that bind membrane receptors or soluble transcription factors and thereby regulate expression from output promoters.[7−9] However, there are several limitations to this approach. First, chemicals can be degraded, absorbed, or modified by cells or the extracellular environment. Because cell density, metabolism, physiology, and media composition can change dynamically during batch culture experiments, microfluidic or continuous culture instruments are needed to maintain chemical signals, and thus gene expression, at desired levels.[10,11] Second, the time scale over which transcription rate can be changed is limited by the rate(s) of import and export of chemical effectors across the cell membrane(s), or the binding and unbinding kinetics with, and downstream signaling from, a receptor. Third, chemical effectors are poorly suited to single- or multicell spatial studies due to diffusion. Finally, the most commonly used chemical effectors are sugars, antibiotics, or growth factors that can be toxic,[12] recognized by alternative receptors,[13] or elicit metabolic, gene regulatory, or physiological responses that can alter expression of the gene(s) of interest in unknown or undesirable ways.[14,15]

Optogenetics is a technology wherein light is used to control molecular biological processes in live organisms via genetically encoded, light-switchable proteins.[16] Over the past 12 years, light-switchable proteins from cyanobacteria, plants, non-photosynthetic bacteria, and humans have been repurposed for synthetic control of gene expression in *E. coli*,[17−20] cyanobacteria,[21] yeast,[22−24] mammalian cells,[23,25−32] zebrafish,[32,33] and within the liver, kidney,[34] and brain[35] of live mice. These sensors are switched from dark-adapted ground to excited states by specific spectral band(s) between the ultraviolet and near-infrared, and revert to the ground state thermally in the dark, or actively in response to a different wavelength.[36] Because light can be delivered to live cells with exacting precision in the wavelength, intensity, temporal, and spatial dimensions, optogenetics dramatically increases the degree of control of biological processes relative to chemical approaches.[37] Moreover, inexpensive microcontrollers and light emitting diodes (LEDs) are sufficient to create quantitatively precise and reproducible optical input signals, even in batch

**Special Issue:** Synthetic Photobiology

**Received:** July 3, 2014
**Published:** September 24, 2014

   dx.doi.org/10.1021/sb500273n | *ACS Synth. Biol.* 2014, 3, 820−831

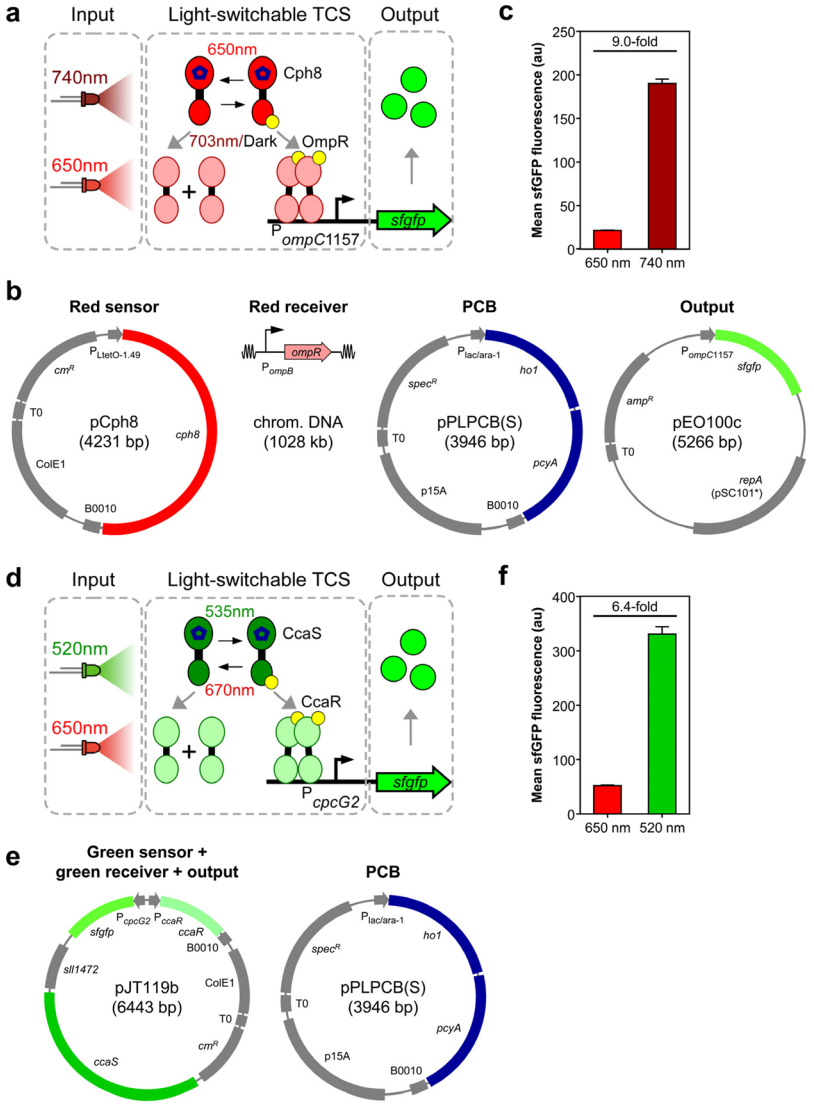


**Figure 1.** Version 1.0 light-switchable *E. coli* two-component systems (TCSs). (a) Cph8-OmpR. Far-red ($\lambda_{max}$ = 740 nm) and red ($\lambda_{max}$ = 650 nm) light emitting diodes (LEDs) are used to create input signals. In the dark-adapted ground state (Pr), PCB (blue pentagons)-ligated Cph8 phosphorylates OmpR, which activates transcription from $P_{ompC1157}$. Red light switches Cph8 from the Pr to Pfr form, which dephosphorylates OmpR ~ P, deactivating transcription. Far-red light or dark reverts Cph8 Pfr to Pr. (b) Plasmid and genomic expression maps of Cph8-OmpR v1.0. (c) Mean sfGFP fluorescence of populations of *E. coli* JT2 carrying Cph8-OmpR v1.0 and illuminated with red or far-red light (Methods). The reported data are the average of three experiments conducted over three separate days. Error bars indicate ± one standard deviation. The ratio of far-red to red GFP fluorescence (fold-activation) is indicated. (d) CcaS-CcaR. Green ($\lambda_{max}$ = 520 nm) and red LEDs are used to create input signals. In the dark-adapted ground state (Pg), PCB-ligated CcaS dephosphorylates CcaR ~ P. Green light exposure switches CcaS Pg to Pr, which autophosphorylates and transfers a phosphoryl group to CcaR, which then activates transcription from $P_{cpcG2}$. Red light reverts CcaS Pr to Pg. (e) Plasmid maps of CcaS-CcaR v1.0. (f) Mean sfGFP fluorescence of *E. coli* BW29655 carrying CcaS-CcaR v1.0 and illuminated with green or red light. Experiments and data representation are as in part C and Methods.

cultures. Finally, because most light-switchable proteins respond to intensities far lower than those commonly used for fluorescent protein imaging,[38] and many nonphotosynthetic model organisms do not show major physiological responses to light, optogenetic perturbations have minimal off-pathway effects.[15]

We have previously engineered two light-switchable two-component signal transduction systems (TCSs) with promoter outputs in *E. coli*.[17,19] The first, named Cph8-OmpR (Figure 1a), was constructed by replacing the N-terminal sensory domain of the *E. coli* sensor histidine kinase (SK) EnvZ with the photosensory core domain (PCD) of the *Synechocystis* PCC 6803 phytochrome Cph1.[17] The hybrid SK Cph1-EnvZ (termed Cph8), which is expressed from the ~50−70 copy ColE1-origin[7] plasmid pCph8 (Figure 1b) (see Supporting Information Table S1 for complete plasmid list), autocatalytically ligates the requisite chromophore phycocyanobilin (PCB) at a conserved cysteine within a GAF (cyclic GMP-binding phosphodiesterase, adenylyl cyclase, FhlA) subdomain of the Cph1 PCD. PCB is produced from heme by coexpression of heme oxygenase 1 (*ho1*) and phycocyanobilin reductase (*pcyA*), also from *Synechocystis* PCC 6803,[39] from the ~20−30 copy p15A-origin[7] plasmid pPLPCB(S) (Figure 1b). Cph8 holoprotein adopts a red light-sensitive ground state, named Pr, wherein the histidine kinase domain phosphorylates the *E. coli* response regulator (RR) OmpR. Phosphorylated OmpR


dx.doi.org/10.1021/sb500273n | *ACS Synth. Biol.* 2014, 3, 820−831

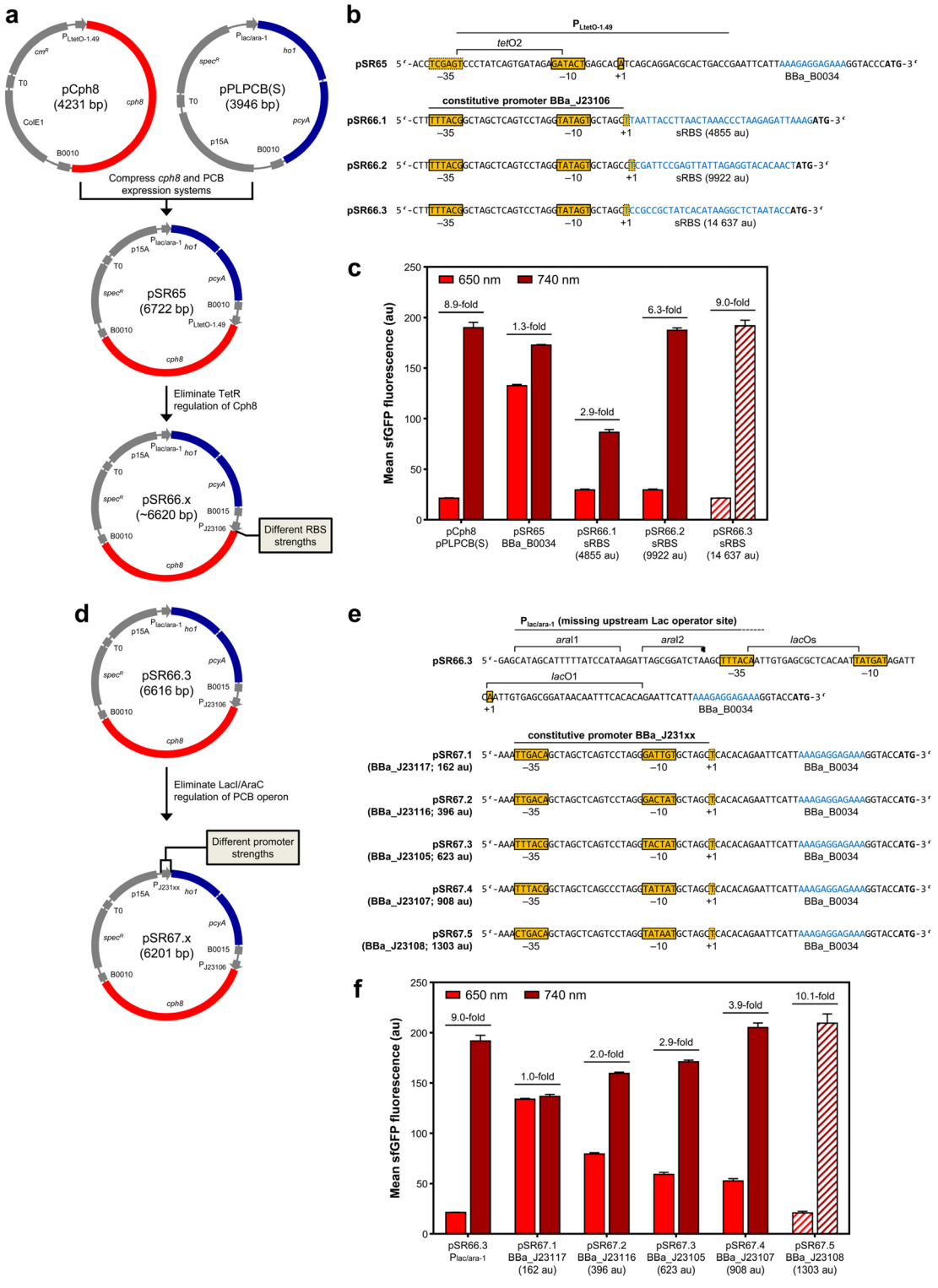


**Figure 2.** Compression and refactoring of *cph8* and *ho1-pcyA* expression plasmids. (a) Plasmid maps. Note that pSR65 and the pSR66 series have reverse backbone orientation relative to pPLPCB(S). (b) Nucleotide sequence of the v1.0 *cph8* promoter and RBS used to refactor *cph8* expression. The promoters are aligned according to the −35 region. RBSs are highlighted in blue, start codons in bold, and dashed boxes indicate BPROM-predicted promoter elements. sRBSs translation strength is shown in arbitrary RBS calculator units (au). (c) R/FR outputs of *E. coli* JT2 carrying the plasmids indicated and pEO100c. Data are reported as in Figure 1. Hashed bars indicate the optimal construct that was carried forward into part D. (d) Compression and refactoring of *ho1-pcyA* expression. (e) Nucleotide sequence of promoters and RBSs used to refactor *ho1-pcyA* expression. DNA annotations are as in part B. The upstream Lac operator site of $P_{lac/ara-1}$[7] is missing in pPLPCB(S). (f) R/FR outputs of *E. coli* JT2 carrying the plasmids shown and pEO100c. Experiments and data representation are as in part C.

(OmpR ~ P) binds to three operator sites within the *ompC* promoter ($P_{ompC}$), activating transcription. Absorption of a red photon converts Cph8 Pr to a far-red absorbing form (Pfr), wherein the kinase domain dephosphorylates OmpR ~ P,


dx.doi.org/10.1021/sb500273n | ACS Synth. Biol. 2014, 3, 820−831

deactivating transcription. Pfr rapidly reverts to Pr upon exposure to far-red light or in the dark.[40] In our most recent and best characterized version of the sensor,[40] an 1157 bp fragment of DNA encoding 107 bp upstream of the *ompC* transcriptional start site, the first 789 bp of *ompC* and several other markers originating from a *lacZ* genomic integration event in the chromosome of the OmpR ~ P reporter strain RU1012[41] (named $P_{ompC1157}$), is used as the output (Figure 1a). $P_{ompC1157}$ activity is read out using a superfolder GFP (*sfgfp*) reporter gene from the 3−4 copy pSC101*-origin[7] plasmid pEO100c (Figure 1b, c).

The second light sensor was engineered by cloning the *Synechocystis* PCC 6803 *ccaS-ccaR-cpcG2* genomic cluster into a ColE1-origin plasmid, and replacing the native *cpcG2* output gene with *sfgfp* (plasmid pJT119b) (Figure 1d, e).[19] CcaS is a SK with a N-terminal PCB-binding cyanobacteriochrome GAF domain and a C-terminal histidine kinase domain.[42] CcaS holoprotein is produced in a green absorbing, phosphatase active ground state (Pg). Green light switches CcaS Pg to a kinase active Pr conformation, where it phosphorylates the RR CcaR. CcaR ~ P binds to a G-box operator within $P_{cpcG2}$,[43] activating transcription. Red light reverts CcaS Pr to Pg, deactivating transcription (Figure 1f).[40]

We have demonstrated that Cph8-OmpR and CcaS-CcaR can be coexpressed and independently controlled in the same cell,[19] and used for exceptionally accurate and precise quantitative,[40] spatial,[17,19] and temporal[40] control of gene expression. Furthermore, by linking Cph8-OmpR to a cell−cell communication system and multiple genetic circuits, we engineered a lawn of *E. coli* to perform the challenging image-processing algorithm of edge detection.[44] Most recently, we used CcaS-CcaR to program sophisticated temporal signals such as sine waves of the transcriptional repressor TetR and used those signals to directly characterize the input/output dynamics of the widely used $P_{LtetO-1}$ promoter in live bacteria.[40] Finally, another group has used CcaS-CcaR to tune *E. coli* growth rate with light by controlling expression of the methionine biosynthetic gene *metE*.[45]

Despite their demonstrated utility, our current light sensors (hereafter version 1.0) suffer several performance limitations. First, in Cph8-OmpR v1.0, *cph8*, *ho1*, *pcyA*, and $P_{ompC1157}$ are distributed across three plasmids, and *ompR* is encoded in the chromosome (Figure 1b). This bulky configuration reduces the capacity of cells carrying Cph8-OmpR to be transformed with other plasmids and restricts the system to strains expressing *ompR*. Second, *cph8* is constitutively transcribed from $P_{LtetO-1}$ in *E. coli* lacking *tetR*, making Cph8-OmpR v1.0 incompatible with strains utilizing *tetR* in genetic circuits or for other purposes. Third, *ho1-pcyA* is transcribed from the LacI-repressed, L-arabinose/AraC-activated promoter $P_{lac/ara-1}$,[7] resulting in cross-talk with strains containing either of these two common transcription factors. Finally, and perhaps most importantly, the system has leaky output in red light (21.22 ± 0.38 arbitrary sfGFP units (au)) and a modest 8.96 ± 0.29-fold activation in far-red light (Figure 1c). Additionally, the CcaS-CcaR v1.0 expression plasmid pJT119b carries the 444 bp *sll1472* gene of unknown function between *ccaS* and $P_{cpcG2}$ (Figure 1e). This system also shows leaky red light output (52.13 ± 1.43 au) and only 6.35 ± 0.31-fold green light activation (Figure 1f).

Here, we use genetic refactoring[46,47] to consolidate Cph8-OmpR onto two plasmids, reduce the overall DNA footprint of both systems, and replace all regulated and native gene expression cassettes with constitutive, well-characterized *E. coli* versions, all while retaining or exceeding the performance of the v1.0 systems (see Supporting Information Figure S1 for overview). By re-engineering output promoters and systematically optimizing the expression levels of both SKs and RRs, we also substantially reduce the leakiness and increase the dynamic range of both TCSs. Because many biological pathways and genetic circuits respond to low levels or specific windows of gene expression, the resulting second-generation light sensors have a wide range of new applications in synthetic and systems biology.

## RESULTS AND DISCUSSION

**Refactoring Cph8-OmpR.** To reduce the number of DNA base pairs, origins of replication, and antibiotic resistance markers associated with Cph8-OmpR, we first moved the *cph8* expression cassette from pCph8 to pPLPCB(S), resulting in pSR65 (Figure 2a, b). We then transformed the *envZ* knockout strain JT2[19] with pSR65 and the pEO100c reporter plasmid (Figure 1b). Bacteria expressing the original or compressed system were grown in exponential phase under saturating red or far-red light using our previously engineered Light Tube Array (LTA) instrument[40] (Methods). We then harvested the cells and quantified sfGFP expression by flow cytometry (Methods). These measurements reveal that pSR65 results in slightly lower pathway output than Cph8-OmpR v1.0 in far-red light but dramatically increased expression in red (Figure 2c) and is thus a poor sensor.

Because we reduced *cph8* gene dosage while moving the expression cassette from a ColE1 to p15A backbone in the construction of pSR65, we hypothesized that higher Cph8 levels may be needed to recover the original light response. To optimize *cph8* expression while simultaneously eliminating TetR cross-talk, we replaced $P_{LtetO-1.49}$ (Supporting Information Note S1) with the constitutively active Anderson collection Biobrick promoter BBa_J23106[48] and replaced the BBa_B0034 ribosome binding site (RBS) with three computationally designed synthetic versions (sRBSs) of increasing strength from 4855 to 14 637 arbitrary RBS calculator units (pSR66 series) (Figure 2b).[49,50] Interestingly, pathway output increases with predicted Cph8 abundance in far-red light, while simultaneously decreasing in red (Figure 2c). Moreover, the strongest sRBS recapitulates both the red and far-red output of Cph8-OmpR v1.0. An immediate explanation for the observed trend is that autophosphorylation from acetyl-phosphate[51] or cross-talk from other SKs[52] results in consistently high OmpR ~ P/OmpR ratios at low Cph8 levels and that Cph8 can override these alternative sources of phosphorylation at higher expression levels.[53] However, deletion of *cph8* results in very low pathway output (Supporting Information Figure S6c), indicating that alternative sources of signaling to OmpR are minimal. Therefore, it is possible that a nonobvious DNA composition effect, such as interference by $P_{LtetO-1.49}$ on transcription of the upstream *ho1-pcyA* operon, resulting in low PCB levels, is responsible for the high leakiness and low dynamic range of pSR65 (see results below).

To further improve pathway performance, we designed two additional pSR66 variants with *cph8* sRBSs strengths of 18 523 and 26 786 au. However, we were unable to construct these plasmids due to the recurrence of spontaneous missense mutations in the *cph8* open reading frame. This outcome agrees with our previous results that high Cph8 levels are strongly selected against during cloning (Supporting Information Note S1), likely due to physiological changes associated with high

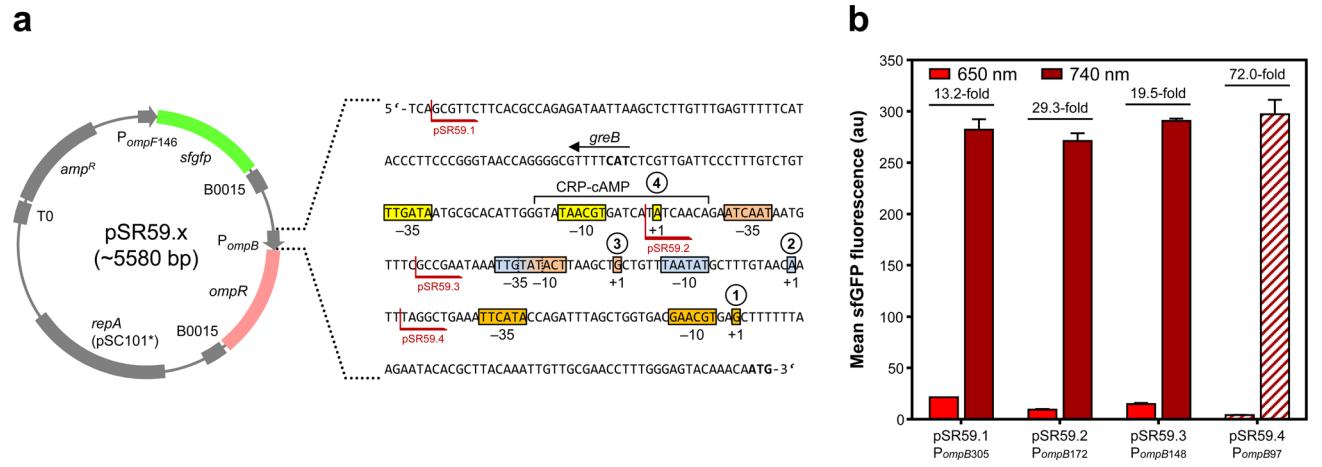


**Figure 3.** Moving *ompR* from the genome to a plasmid and optimizing the promoter. (a) *ompR* was cloned under control of different versions of the native *ompB* promoter ($P_{ompB}$) on plasmids pSR59.1−59.4, which contain the optimized output promoter $P_{ompF146}$ (Supporting Information Note S3, Figure S3) driving *sfgfp*. The sequence of the 305 nucleotides upstream of *ompR* is shown with promoters numbered according to their distance from the start codon (bold). This region was chosen because it contains all four *ompB* promoters plus an additional 100 bp. The CRP-cAMP operator is indicated. For clarity, three IHF operators are not depicted. The direction of the upstream *greB* open reading frame is indicated by an arrow, with the start codon in bold. Open red brackets show the starting position of truncated promoters in the corresponding plasmid. (b) R/FR outputs of *E. coli* BW29655 carrying the plasmids and $P_{ompB}$ variants indicated and the *cph8* and PCB expression plasmid pSR33.4. Data represented as in Figure 2c.

OmpR ∼ P or cross-talk of the EnvZ histidine kinase domain with other RRs.[54]

After eliminating pCph8 and cross-talk with TetR, we set out to replace $P_{lac/ara-1}$ with a constitutive promoter. Because sensor performance is likely to be sensitive to PCB levels, we constructed a series of plasmids wherein *ho1-pcyA* is expressed from one of five Anderson collection promoters of different strengths (pSR67 series) (Figure 2d, e) and tested the light response of each as above. For the weakest promoter (BBa_J23117, 162 arbitrary Anderson promoter units (au)), the pathway is nonlight switchable, with relatively high far-red and red output levels resembling to those observed for pSR65 (Figure 2f). Mirroring the trend observed for Cph8, higher predicted PCB levels result in both higher far-red and lower red light output and therefore greater dynamic range (Figure 2f). The strongest promoter tested (BBa_J23108, 1303 au, pSR67.5) results in a 10.06 ± 0.87-fold dynamic range, a slight improvement over Cph8-OmpR v1.0. We attempted to further improve pathway performance by cloning stronger promoters (BBa_J23118, 1429 au; BBa_J23101, 1791 au), but all successfully assembled plasmids contain spontaneous mutations in *ho1* or the promoters themselves, suggesting that pSR67.5 drives production of a near maximal (and optimal) level of PCB without causing toxicity due to heme depletion (Supporting Information Note S4, Figure S7).

Taken together, the *ho1-pcyA* expression optimization data (Figure 2f) indicate that Cph8 kinase, phosphatase, and light-switching activity are all stimulated by PCB. Additionally, the fact that pathway output in red light is more sensitive to PCB levels than far-red implies that apo-Cph8 has a higher kinase than phosphatase activity, relative to the corresponding holo-Cph8 state.

**Identification of a Novel Cph8 Mutation and *ompF* Output Promoter Variant That Improve Sensor Performance.** Two mutations, I650V and T740M, arose within the EnvZ catalytic and ATPase (CA) domain during the original construction of pCph8[17] (Supporting Information Figure S2a, b) and are present in all *cph8*-bearing plasmids that we have reported to this point. We also observed a novel CA domain mutation, G722V (Supporting Information Figure S2b), alongside I650V and T740M during the *cph8* refactoring above (see Supporting Information Note S2 for detailed description), though G722V is not present in any experiment to this point. To examine the possibility that one or more of these mutations impacts Cph8 function, we constructed pSR67.5 variants encoding *cph8* carrying a nonmutated EnvZ domain, and each of the three single mutations (pSR33 series), and compared the corresponding light responses to the published Cph8 sequence. First, the wild-type sequence yields slightly higher dynamic range than the published version (13.62 ± 0.38 versus 10.06 ± 0.87-fold) due to lower leakiness (Supporting Information Figure S2c). Additionally, while both published mutations are slightly deleterious, G722V improves dynamic range over wild-type to 19.17 ± 0.94-fold, due to lower red light output (Supporting Information Figure S2c). Similar to their effect on the wild-type, either or both of the published mutations reduces the dynamic range and increases the leakiness of the G722V mutant. Based on its improved performance features, we chose to carry *cph8* G722V (hereafter *cph8**) forward for all subsequent experiments.

To continue to improve sensor performance while reducing the DNA footprint, we next aimed to replace $P_{ompC1157}$ (Supporting Information Figure S3a) with a shorter promoter lacking unwanted regulatory elements and additional transcription start sites. To this end, we constructed a small library of truncations of $P_{ompC}$ as well as of $P_{ompF}$, a second OmpR ∼ P activated promoter, wherein one or more elements flanking the core OmpR operators is deleted in each variant (Supporting Information Note S3, Figure S3b−e). While most truncations perform more poorly, $P_{ompF146}$, a 146 bp variant deleted for the region upstream of the OmpR operators and a second predicted constitutive promoter has higher dynamic range than $P_{ompC1157}$ (30.55 ± 1.06 versus 19.17 ± 0.94-fold) while retaining low red light leakiness (Supporting Information Figure S3e). We therefore replaced $P_{ompC1157}$ with $P_{ompF146}$ in all following experiments.

**Optimizing *ompR* Expression Level.** To optimize *ompR* expression while making Cph8-OmpR more modular and


dx.doi.org/10.1021/sb500273n | ACS Synth. Biol. 2014, 3, 820−831

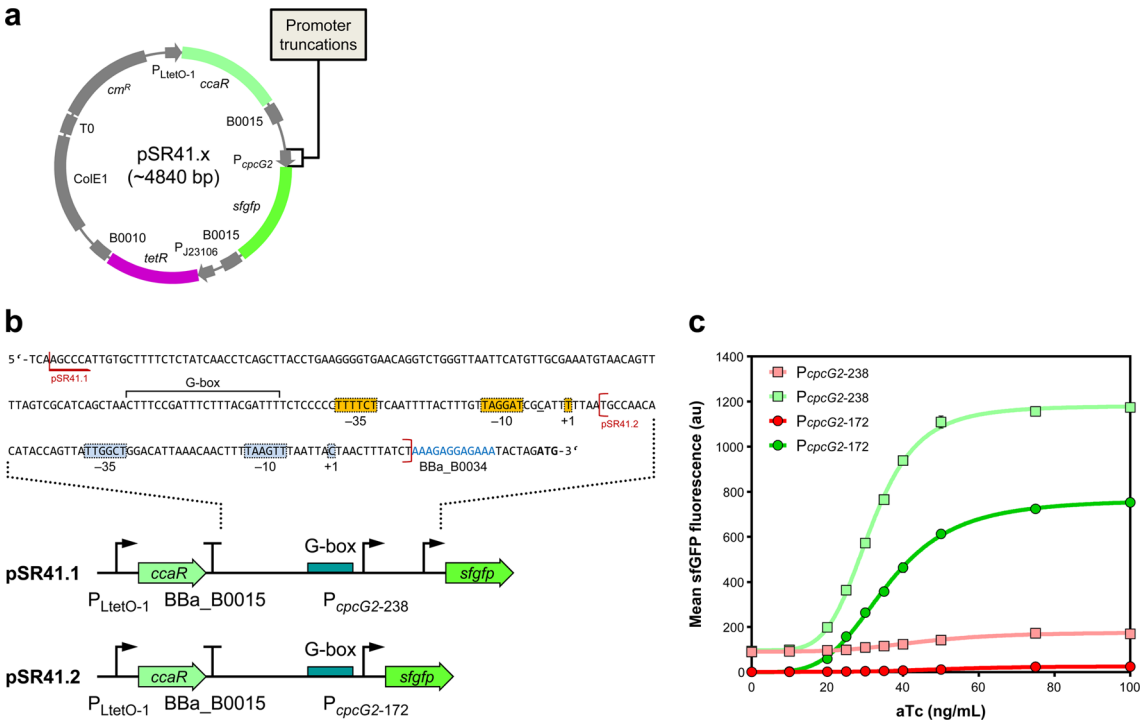


**Figure 4.** Reducing the leakiness and increasing the dynamic range of $P_{cpcG2}$. (a) The pSR41 series plasmid design. (b) The BPROM predicted elements of the CcaR ∼ P regulated promoter are shown in yellow. Those of the putative constitutive promoter are shown in blue. The experimentally identified transcription start site of $P_{cpcG2}$ in *Synechocystis* PCC 6803[67] is underlined, and the *sfgfp* start codon is shown in bold. The long, open red bracket indicates the starting position of $P_{cpcG2\text{-}238}$ in pSR41.1, while the short closed brackets bind the region lacking in $P_{cpcG2\text{-}172}$ (pSR41.2). (c) sfGFP output of *E. coli* BW29655 carrying the optimized *ccaS* and PCB expression plasmid pSR43.6 and pSR41.1 (□) or pSR41.2 (○) illuminated with red (red lines) or green (green lines) light and supplemented with different anhydrotetracycline (aTc) concentrations. Growth experiments and gene expression analysis are as described in Methods. Each data point indicates the mean of three experiments conducted over three separate days. Error bars indicate ± one standard deviation.

portable, we next set out to move *ompR* from the genome to a plasmid. In *E. coli*, *ompR* and *envZ* are expressed from the *ompB* operon, which is transcribed from four promoters (Figure 3a).[55,56] For plasmid-based *ompR* expression, we first changed the host strain to BW29655, a derivative of *E. coli* K-12 BW25113 lacking both *ompR* and *envZ*.[57] BW29655 was cotransformed with pSR33.4, containing the refactored and optimized *cph8** and PCB expression cassettes (Supporting Information Figure S2) and one of four plasmids encoding *sfgfp* under $P_{ompF146}$ and *ompR* under a $P_{ompB}$ truncation variant containing all four, three, two, or one of the native promoters (Figure 3a) (pSR59 series). Despite the increased *ompR* dosage, all pSR59 plasmids result in approximately 40% lower far-red light output in BW29655 than the comparable engineered pathway in JT2 (Figure 3b and Supporting Information Figure S3e). In contrast, red light output changes with the number of *ompB* promoters, with expression ranging from 21.34 ± 0.03 au for all four promoters to as low as 4.13 ± 0.12 au for $P_{ompB97}$, which contains only the *ompR*-proximal promoter (Figure 3b). Due to this combination of low leakiness and high activated expression level, $P_{ompB97}$ results in a markedly improved 71.98 ± 3.99-fold dynamic range. Using Anderson collection promoters, we were unable to achieve the dynamic range observed with $P_{ompB97}$ (data not shown). However, because $P_{ompB97}$ is to our knowledge unregulated, all pathway components are constitutively expressed from pSR33.4 and pSR59.4 (hereafter Cph8-OmpR v2.0).

There are several benefits to Cph8-OmpR v2.0. First, unlike the v1.0 system, it is compatible with strains encoding *tetR*, *lacI*, or *araC*. Moreover, because the ColE1 origin and the chloramphenicol resistance marker have been eliminated, and the size is reduced by ∼20% (11 564 versus 14 471 bp), Cph8-OmpR v2.0 can be readily combined with larger plasmid-borne synthetic genetic systems. In addition, low leakiness and high dynamic range make this second generation sensor better suited to the expression of toxic proteins such as the CRISPR interference (CRISPRi)[58]-associated dCas9 or repressors such as small guide RNAs (sgRNAs)[58] or λCI that have low $K_d$ values for target promoters.[44,59] Moreover, because all DNA is encoded on two plasmids, this system can more readily be ported to other strains, or possibly other bacteria, including those lacking genomic *ompR*. Full plasmid encoding also makes Cph8-OmpR v2.0 convenient for engineering synthetic signaling pathways[60−66] based upon Cph8, OmpR, or any of their subdomains.

**Refactoring and Optimization of CcaS-CcaR.** Our previous work with CcaS-CcaR has been conducted in *E. coli* JT2.[19,40] However, because this TCS is not native to *E. coli*, it should function in most any strain, assuming minimal cross-talk with native TCSs and genomic promoters. We therefore chose to refactor and optimize CcaS-CcaR in BW29655, the same strain used to engineer Cph8-OmpR v2.0. In this strain, CcaS-CcaR v1.0 produces 52.13 ± 1.43 and 330.88 ± 13.55 au of sfGFP in red and green light, corresponding to 6.35 ± 0.31-fold activation (Figure 1f). We note that absolute sfGFP output from the ColE1 origin pJT119b is greater than that from the pSC101* reporter plasmids used for Cph8-OmpR, necessitating the use of lower cytometer gain settings (Supporting


dx.doi.org/10.1021/sb500273n | ACS Synth. Biol. 2014, 3, 820−831

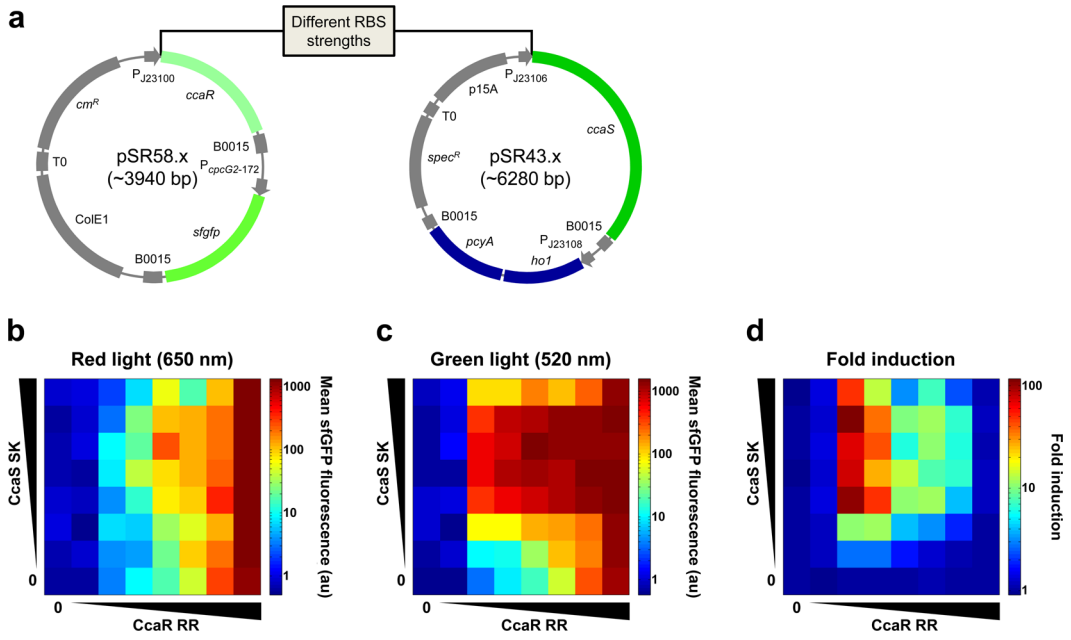


**Figure 5.** Optimizing *ccaS* and *ccaR* expression levels. (a) Plasmid maps of "hard-wired" *ccaS* and *ccaR* tunable expression systems. (b–d) *E. coli* BW29655 was cotransformed with different combinations of the pSR58 and pSR43 series and controls lacking either SK or RR (pSR34 and pSR63, respectively). See Supporting Information Table S3 for a detailed list of plasmid combinations used in this experiment. Cells were illuminated with red or green light and sfGFP expression was measured as described in Methods. Each data point indicates the mean of three experiments conducted over three separate days. Fluorescence (b and c) and fold induction (d) values are summarized in Supporting Information Table S9.

Information Table S2) and therefore different arbitrary fluorescence units for the two systems.

In CcaS-CcaR v1.0, we utilize the full 238 bp region between *cpcG2* and *ccaR* as the $P_{cpcG2}$ output promoter. Recently, the *cpcG2* transcriptional start site was determined to be 75 bp upstream of the start codon in *Synechocystis* PCC 6803.[67] However, the transcriptional start site(s) may differ in *E. coli*. Therefore, we used BPROM[68] to predict *E. coli* $\sigma^{70}$ promoters between the G-box, which resides near the center of the intergenic region, and *sfgfp* (Supporting experimental procedures). This analysis reveals a promoter with a −35 hexamer that begins 8 bp downstream of the G-box, in agreement with the *Synechocystis* start site. However, we also identify a second putative promoter with a −35 hexamer starting 66 bp downstream, near *sfgfp* (Figure 4a, b). Because of its proximity to the G-box, we hypothesized that the first promoter is activated by CcaR ~ P and responsible for green light activation in *E. coli*. Alternatively, due to the absence of identifiable operator sites nearby, we hypothesized that the second putative promoter is constitutive and contributes to leakiness and low dynamic range.

To examine these hypotheses, we constructed pSR41.1 and pSR41.2, which contain full length $P_{cpcG2}$ (hereafter $P_{cpcG2\text{-}238}$) and a truncated version deleted for the second candidate promoter ($P_{cpcG2\text{-}172}$), respectively. To measure the response of both promoters to CcaR ~ P, the pSR41 series was also engineered to carry an aTc-inducible *ccaR* cassette (Figure 4a, b). For analysis, BW29655 was cotransformed with pSR41.1 or pSR41.2 and a variant of the optimized *ho1-pcyA* expression plasmid pSR67.5 with a constitutive *ccaS* expression cassette in place of *cph8* (pSR43.6) (Supporting Information Figure S4). Bacteria carrying these plasmids were grown in red or green light in the presence of aTc between 0 and 100 ng/mL. Without aTc, neither $P_{cpcG2\text{-}238}$ nor $P_{cpcG2\text{-}172}$ is induced by green light (Figure 4c), indicating that *ccaR* is tightly repressed by TetR. Additionally, $P_{cpcG2\text{-}238}$ produces a large amount of leaky transcription at 0 ng/mL aTc in red light (89.29 ± 3.14 au), while $P_{cpcG2\text{-}172}$ produces exceptionally little (0.66 ± 0.03 au). Both promoters show a large sigmoidal increase in transcription as a function of aTc in green light but a much smaller increase in red (Figure 4c).

Taking the ratio of the green and red aTc dose–response curves (transfer functions), we observe a maximum $P_{cpcG2\text{-}172}$ dynamic range of 68.76 ± 3.84-fold near 30 ng/$\mu$L and a decrease thereafter (Supporting Information Figure S5). Due to higher red light output levels, we observe a much smaller maximum dynamic range of 7.80 ± 0.27-fold from $P_{cpcG2\text{-}238}$ (Supporting Information Figure S5). The nonmonotonic activation of $P_{cpcG2\text{-}172}$ may occur due to saturation of the promoter by CcaR ~ P at intermediate CcaR expression levels in green light, combined with CcaR ~ P levels that remain well below the saturation point in red. RR ~ P levels have also been shown to saturate despite increasing concentrations of total RR, depending on the properties of the specific TCS.[69,70] It is therefore possible that CcaR ~ P reaches a maximum level at intermediate aTc concentrations, while total CcaR continues to increase with higher aTc concentrations. In either case, the large difference between the green and red light aTc transfer functions indicates that CcaS Pg maintains low CcaR ~ P over a wide range of total CcaR levels. Additionally, the aTc transfer function data support a model that the G-box proximal $P_{cpcG2\text{-}238}$ promoter is strongly activated by CcaR ~ P, while the second, distal promoter is constitutive and responsible for the leakiness and low dynamic range of CcaS-CcaR v1.0 in *E. coli*.

Given its markedly improved performance, we next set out to incorporate $P_{cpcG2\text{-}172}$ into a "hard-wired" v2.0 system wherein *ccaS* and *ccaR* are constitutively expressed to optimal levels. To this end, we deleted the *tetR* expression cassette from pSR41.2 and replaced $P_{LtetO\text{-}1}$ with the strongest Anderson collection promoter BBa_J23100 (2547 au). To vary *ccaR* expression, we


dx.doi.org/10.1021/sb500273n | *ACS Synth. Biol.* 2014, 3, 820–831

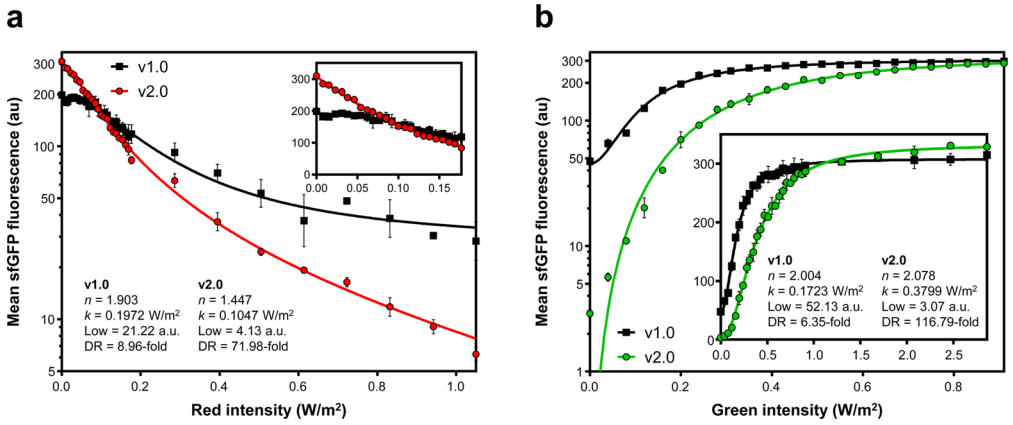


**Figure 6.** Comparison of v1.0 and v2.0 system steady state transfer functions. (a) The sfGFP output of Cph8-OmpR v1.0 (squares) and 2.0 (circles) in response to red light in the presence of 1.38 W/m$^2$ far-red. For v1.0, *E. coli* JT2 carries the plasmids in Figure 1c. For v2.0, *E. coli* BW29655 carries the plasmids in Supporting Information Figure S6b. Cultures are grown and data collected as in Methods. Each data point indicates the mean of three experiments conducted over three separate days. Error bars indicate ± one standard deviation. The data are fit to the repressing Hill function $[a - (b * I_r^n)/(k^n + I_r^n)]$. Low indicates leaky output. DR indicates dynamic range. For a complete list of fit parameters and uncertainties, see Supporting Information Table S4. Inset shows the enlarged region of low red intensities. (b) The response of CcaS-CcaR v1.0 (squares) and 2.0 (circles) to green light in response to 1.05 W/m$^2$ red. For v1.0, *E. coli* BW29655 carries the plasmids in Figure 1e. For v2.0, this strain carries the plasmids listed in Supporting Information Figure S6e. Experiments were conducted as in Methods. Data representation and error bars are as in part A. The data are fit to the activating Hill function $[a + (b * I_g^n)/(k^n + I_g^n)]$. For a complete list of fit parameters and uncertainties, see Supporting Information Table S5. Inset shows the full range green intensity using the LTA.

used 18 sRBSs with strengths between 97 and 961 au in the pSR58 series (Figure 5a). To tune *ccaS* expression, we constructed a 17-member sRBS library (pSR43 series) with translation initiation rates ranging from 5380 to 49 251 au.

Each pSR58 and pSR43 member was cotransformed with pSR43.5 or pSR58.6, respectively, and the response to red and green light prescreened (data not shown). Based upon the prescreening data, we selected seven *ccaS* and seven *ccaR* sRBS variants with widely different expression levels for more detailed characterization. Specifically, we cotransformed seven pSR58 variants and a plasmid deleted for *ccaS* against seven pSR43 variants and a plasmid lacking *ccaR* (Supporting Information Table S3). We then grew each of the 64 strains under red and green light and analyzed pathway output as a function of CcaR and CcaS level. To interpret CcaR levels, we simply use sfGFP output in either light condition, which increases monotonically with *ccaR* expression (Figure 4c). To measure the CcaS level, we constructed a series of analytical plasmids wherein *sfgfp* is fused C-terminally to the first 12 amino acids of *ccaS* (pSR76 series) and used measured sfGFP fluorescence as a proxy for CcaS level (Supporting Information Figure S4b).

We then plotted the red and green light pathway outputs and fold induction in two-dimensional heat maps wherein the 64 plasmid combinations are ordered by the expression levels of the SK and RR (Figure 5b–d). Though several groups have analyzed TCS performance while varying one or both pathway components over ranges of variable magnitude,[64,69−71] these data represent the first study where the expression levels of a natural SK and RR have been systematically varied against one another. This analysis reveals several interesting pathway properties. First, in agreement with our previous measurements (Figure 4c), sfGFP is low in both red and green light at very low CcaR levels (Figure 5b, c). Additionally, pathway output increases with CcaR abundance in both red and green, regardless of the CcaS level (Figure 5b, c). This increase occurs in cells lacking *ccaS* as well, suggesting that CcaR autophosphorylates, is phosphorylated to a small extent by other *E. coli* SKs in the absence of CcaS,[43] or binds DNA weakly in the nonphosphorylated form.[72] For the highest CcaR levels, we observe that pathway output is high in both red and green light, regardless of *ccaS* expression level (Figure 5b, c). In our aTc-inducible *ccaR* experiments, red light output remains much lower than green at all aTc levels despite a stronger predicted *ccaR* RBS, suggesting that transcription from BBa_J23100 is stronger than that of $P_{LtetO-1}$.

Not surprisingly, the pathway is not strongly activated by green light at low CcaS levels. However, pathway switching is relatively insensitive to CcaS abundance, with consistently strong green light activation when CcaS is above the lowest levels tested (Figure 5d). Unexpectedly, output again decreases at the highest CcaS levels (Figures 5b–d, top row). This effect occurs more strongly in green than red light, resulting in lower fold activation and thus an optimal intermediate CcaS concentration range. One possibility is that PCB becomes limiting when total CcaS is high, creating a population of apo-CcaS molecules with constitutive ground state phosphatase activity. Such a population would have a greater impact on CcaR ~ P/CcaR ratio in the presence of kinase-active Pr form holo-CcaS than phosphatase active Pg form. Finally, the heat map data reveal that the combination of pSR43.6 and pSR58.6 results in the highest green light activation yet observed (116.79 ± 5.95-fold) and low leakiness (Figure 5b, d, second column, third row). Hereafter, we refer to this combination of plasmids as CcaS-CcaR v2.0.

**Characterizing the v2.0 Light Sensors.** Using the v1.0 sensors, the single cell transcription rate can be precisely tuned by varying the intensity of the ground state-responsive wavelength (red for Cph8-OmpR, green for CcaS-CcaR).[40] Furthermore, for CcaS-CcaR, we have observed that the presence of the competing wavelength (red) reduces the steepness of the transfer function while preserving the full dynamic range, permitting finer analog control of the transcription rate.[40]

To compare the quantitative relationship between input and output of the v1.0 and v2.0 systems, we next characterized their


dx.doi.org/10.1021/sb500273n | ACS Synth. Biol. 2014, 3, 820−831

steady state transfer functions. Bacteria expressing Cph8-OmpR v1.0 and v2.0 (Supporting Information Figure S6a–c) were grown under different red intensities from 0.00 to 1.05 W/m$^2$, with a far-red constant at 1.38 W/m$^2$. Our measurements reveal that output decreases proportionally to red intensity in a manner described by a repressing Hill function for both versions of the sensor (Figure 6a). However, there are several notable differences. First, v2.0 has a lower response threshold, with half-maximal deactivation ($k$) occurring at approximately half the intensity of v1.0 (0.105 versus 0.197 W/m$^2$) (Supporting Information Table S4). Additionally, the v1.0 transfer function is sigmoidal, with a shallow response to red light intensities of less than 0.10 W/m$^2$ followed by a steeper response and saturation (Hill parameter $n$ = 1.90). By contrast, Cph8-OmpR v2.0 responds sharply to low red intensities, resulting in a more hyperbolic transfer function ($n$ = 1.45) (Figure 6a). These data suggest in far-red light for v1.0, OmpR ~ P or $P_{ompC1157}$ are saturated, requiring a relatively large increase in EnvZ phosphatase activity to elicit a transcriptional response, while OmpR ~ P or $P_{ompF146}$ is not saturated in v2.0, resulting in a sensitive response to low red light intensities. This interpretation also suggests that yet higher pathway output and greater dynamic range could still be achieved.

To characterize the CcaS-CcaR v2.0 (Supporting Information Figure S6d–f) transfer function, we varied green light intensity from 0.00 to 2.86 W/m$^2$ in the presence of 1.05 W/m$^2$ red. In contrast to Cph8-OmpR, CcaS-CcaR v2.0 has a higher response threshold ($k$ = 0.380 versus 0.172 W/m$^2$), but the transfer function retains the same steepness ($n$ = 2.08 versus 2.00) (Figure 6b and Supporting Information Table S5). The reduced green light sensitivity enables the user to program more analog outputs, especially very low levels, from CcaS-CcaR v2.0. The ability to fine-tune low levels of gene expression is a feature lacking in v1.0 (Figure 6b).

**Conclusions.** In this study, we have dramatically improved the user-friendliness and performance features of the Cph8-OmpR and CcaS-CcaR light-switchable TCSs, two of the best-characterized and controllable optogenetic tools in the literature. The first generation versions of these sensors have several notable limitations, including bulky plasmid and DNA encoding, limited portability, cross-talk with common transcription factors, leaky transcription, and modest dynamic range. The second generation engineered here overcomes all of these issues, with complete and compact plasmid encoding, the exclusive use of constitutive promoters for expression of pathway genes, dramatically reduced leakiness, and upward of or exceeding 100-fold dynamic range. As a result, the second generation light sensors can be combined with more (and larger) plasmid-borne synthetic genetic systems and circuits and used to characterize those systems over a wider range of gene expression, in particular, at low levels. In synthetic and systems biology applications, low expression is particularly useful for metabolic enzymes, toxic proteins, proteins such as Cas9 with high off target effects, or strong transcription factors such as the dCas9:sgRNA complexes of the CRISPRi technology.

TCSs are the primary means by which bacteria sense and respond to their environment.[73] More than 75 000 TCSs have been identified computationally,[74] and these pathways could be used to engineer novel biological sense-respond functions such "synthetic probiotics" that diagnose and treat diseased states in the body.[75−77] However, as observed for our light sensors, TCSs taken largely "as-is" from nature may show suboptimal performance features, limiting their utility for synthetic biology. The TCS performance optimization approach that we demonstrate here will therefore be key to future synthetic biology applications. Our two-pronged approach of systematic optimization of pathway component expression levels and re-engineering of evolved output promoters may also be extensible to eukaryotic systems such as MAP kinase pathways, thus enabling the engineering of sensors of a wide range of important cellular input signals.

## METHODS

**Growth Conditions, Strains, and Plasmids.** All experiments were performed using *E. coli* strain JT2 (RU1012, $\Delta P_{ompC}$-*lacZ*)[19] or BW29655 (BW28357 Δ(*envZ-ompR*)*520*-(::*FRT*)).[57] LB Miller broth was used as standard medium for cultivation of the bacteria. Cells were grown under agitation (250 rpm) at 37 °C. As appropriate, antibiotics were added to the medium (50 μg/mL ampicillin, 34 μg/mL chloramphenicol, and/or 100 μg/mL spectinomycin). All *E. coli* JT2 strains were grown in media supplemented with 50 μg/mL kanamycin. Glycerol stocks of all strains were made by adding 300 μL 60% glycerol to 700 μL actively growing culture (log phase) and freezing at −80 °C. For all light exposure experiments, *E. coli* were grown in M9 minimal medium containing 1× M9 salts, 0.4% (wt/vol) glucose, 0.2% (wt/vol) casamino acids, 2 mM $MgSO_4$, 0.1 mM $CaCl_2$, and the appropriate antibiotics.

DNA construction was carried out in *E. coli* strain NEB 10-β (New England Biolabs, catalog no. C3019H) following standard procedures.[78] The plasmids and primers used in this study are listed in Supporting Information Tables S1 and S6, respectively. For plasmid construction, DNA fragments were amplified using the primers listed in Supporting Information Table S7. PCR products were individually gel-purified from 1% agarose using the Wizard SV Gel and PCR Clean-Up System (Promega, catalog no. A9282) and the concentration determined with a NanoDrop 2000 (Thermo Fisher Scientific, Waltham, MA, U.S.A.). Golden Gate assembly[79] was used to construct the final plasmids utilizing type II endonuclease *Bsa*I. For one-part Golden Gate assemblies, the template vector was linearized by PCR-amplification resulting in the replacement of specific DNA elements (promoters or synthetic RBSs) by primer overhangs as well as the introduction of desired truncations (see Supporting Information Table S7 for detailed description). All plasmid constructs were confirmed by sequencing at Lone Star Laboratories, Inc. (Houston, TX, U.S.A.).

**Light Exposure Experiments.** Light exposure experiments were performed using the LTA.[40] Starting from a −80 °C glycerol stock, strains were inoculated into 3 mL LB Miller Broth in culture tubes (BD Biosciences, catalog no. 352006) containing the relevant antibiotics, and grown at 37 °C and 250 rpm for 13 h. Cultures were then diluted 10-fold into 1 mL fresh LB Miller Broth and the $OD_{600}$ determined using a Cary50 UV/vis spectrophotometer (Agilent, Inc.). Cells were then further diluted ($OD_{600}$ 0.0005, or $OD_{600}$ 0.00015 for strains harboring the weaker PCB expression plasmids, pSR67.1−4) in 3 mL M9 minimal medium in culture tubes containing the appropriate antibiotics. For induction of genes under the control of $P_{LtetO-1}$, aTc was added to bring the medium to a concentration in the range between 0 and 100 ng/mL. The tubes were placed in the LTA and incubated at 37 °C, 250 rpm, under the prescribed light condition (red = 650 nm, 1.05 W/m$^2$; far-red = 740 nm, 1.38 W/m$^2$; green = 520 nm,


dx.doi.org/10.1021/sb500273n | ACS Synth. Biol. 2014, 3, 820−831

4.03 W/m$^2$) for an additional 6.5 (BW29655) or 7 h (JT2) for Cph8-OmpR and 8 h for CcaS-CcaR, reaching a final $OD_{600}$ ~0.3 (exponential growth phase; see Supporting Information Note S4, Figure S7, for v1.0 and v2.0 system growth rate comparison). All culture tubes were immediately transferred into an ice water bath and incubated for 45 min before being diluted 50-fold into 1 mL phosphate buffered saline for flow cytometry analysis.

**Flow Cytometry and Analysis.** Flow cytometry acquisition was performed using a BD FACScan (BD, Franklin Lakes, NJ, U.S.A.) with the original laser system replaced by blue (488 nm, 30 mW) and yellow (561 nm, 50 mW) solid-state lasers (Cytek). The FL1 (sfGFP) acquisition channel emission filter was also replaced with a 510/21 nm filter. The cytometer is calibrated using beads (Spherotech, catalog no. RCP-30-5A) on a weekly basis. Acquisition was performed with typical count rates of 1000−2000 events/s. Approximately 50 000 events are stored for each sample. A SSC threshold is used to eliminate instrument noise events that are not due to cell scattering. The cytometer settings used for the acquisition of fluorescence data are listed in Supporting Information Table S5. Representative histograms of single-cell populations are shown in Supporting Information Figures S8 and S9.

For data analysis, events were gated using Flowing Software v2.5.1 (Cell Imaging Core, Turku Centre for Biotechnology, Finland). A small elliptical gate centered at the median FSC and SSC values was used to isolate a uniformly sized population of cells. The gating procedure leaves around 10 000−15 000 events. In addition, a trim was performed on FL1 to remove a small number of apparent noncellular events. The geometric means of the fluorescence distributions were calculated. The autofluorescence value of *E. coli* JT2 or BW29655 cells harboring no plasmid (strain JT2, 9.78 ± 0.24 au; strain BW29655, 1.43 ± 0.07 au and 17.62 ± 0.32 au for gain setting 500 and 800, respectively) was subtracted from these values to give the fluorescence data reported in this study (Supporting Information Tables S8−10).

## ■ ASSOCIATED CONTENT

### Supporting Information

Additional notes, experimental procedures, figures, and tables. This material is available free of charge via the Internet at http://pubs.acs.org.

## ■ AUTHOR INFORMATION

### Corresponding Author

*Email: jeff.tabor@rice.edu.

### Notes

The authors declare no competing financial interests.

## ■ ACKNOWLEDGMENTS

We thank Evan Olson for helpful discussions. We thank Adam Ayoub and Devon Stork for assistance with early experiments. This research was supported by the U.S. National Science Foundation Biotechnology, Biochemical, and Biomass Engineering (BBBE) program (EFRI-1137266) and the Office of Naval Research MURI program (N000141310074). J.J.T. is supported by the Defense Advanced Research Projects Agency Living Foundries Advanced Tools and Capabilities for Generalizable Platforms (ATCG), and ONR Young Investigator Programs. S.R.S is supported by a research fellowship from the Deutsche Forschungsgemeinschaft (DFG) (SCHM 2971/1-1).

## ■ REFERENCES

(1) Tu, B. P., Kudlicki, A., Rowicka, M., and McKnight, S. L. (2005) Logic of the yeast metabolic cycle: Temporal compartmentalization of cellular processes. *Science 310*, 1152−1158.

(2) Payne, S., Li, B., Cao, Y., Schaeffer, D., Ryser, M. D., and You, L. (2013) Temporal control of self-organized pattern formation without morphogen gradients in bacteria. *Mol. Syst. Biol. 9*, 697.

(3) Levine, J. H., Lin, Y., and Elowitz, M. B. (2013) Functional roles of pulsing in genetic circuits. *Science 342*, 1193−1200.

(4) Cai, H., Katoh-Kurasawa, M., Muramoto, T., Santhanam, B., Long, Y., Li, L., Ueda, M., Iglesias, P. A., Shaulsky, G., and Devreotes, P. N. (2014) Nucleocytoplasmic shuttling of a GATA transcription factor functions as a development timer. *Science 343*, 1249531.

(5) Olson, E. J., and Tabor, J. J. (2012) Post-translational tools expand the scope of synthetic biology. *Curr. Opin. Chem. Biol. 16*, 300−306.

(6) Ang, J., Harris, E., Hussey, B. J., Kil, R., and McMillen, D. R. (2013) Tuning response curves for synthetic biology. *ACS Synth. Biol. 2*, 547−567.

(7) Lutz, R., and Bujard, H. (1997) Independent and tight regulation of transcriptional units in *Escherichia coli* via the LacR/O, the TetR/O and AraC/$I_1$-$I_2$ regulatory elements. *Nucleic Acids Res. 25*, 1203−1210.

(8) Weber, W., and Fussenegger, M. (2007) Inducible product gene expression technology tailored to bioprocess engineering. *Curr. Opin. Biotechnol. 18*, 399−410.

(9) Liang, J., McLachlan, M. J., and Zhao, H. (2013) Orthogonal control of endogenous gene expression in mammalian cells using synthetic ligands. *Biotechnol. Bioeng. 110*, 1419−1429.

(10) Menolascina, F., Fiore, G., Orabona, E., De Stefano, L., Ferry, M., Hasty, J., di Bernardo, M., and di Bernardo, D. (2014) *In-vivo* real-time control of protein expression from endogenous and synthetic gene networks. *PLoS Comput. Biol. 10*, e1003625.

(11) Takahashi, C. N., Miller, A. W., Ekness, F., Dunham, M. J., and Klavins, E. (2014) A low cost, customizable turbidostat for use in synthetic circuit characterization. *ACS Synth. Biol.*, DOI: 10.1021/sb500165g.

(12) Xie, J., Nair, A., and Hermiston, T. W. (2008) A comparative study examining the cytotoxicity of inducible gene expression system ligands in different cell types. *Toxicol. In Vitro 22*, 261−266.

(13) Toettcher, J. E., Weiner, O. D., and Lim, W. A. (2013) Using optogenetics to interrogate the dynamic control of signal transmission by the Ras/Erk module. *Cell 155*, 1422−1434.

(14) Uhlendorf, J., Miermont, A., Delaveau, T., Charvin, G., Fages, F., Bottani, S., Batt, G., and Hersen, P. (2012) Long-term model predictive control of gene expression at the population and single-cell levels. *Proc. Natl. Acad. Sci. U.S.A. 109*, 14271−14276.

(15) Olson, E. J., and Tabor, J. J. (2014) Optogenetic characterization methods overcome key challenges in synthetic and systems biology. *Nat. Chem. Biol. 10*, 502−511.

(16) Deisseroth, K. (2011) Optogenetics. *Nat. Methods 8*, 26−29.

(17) Levskaya, A., Chevalier, A. A., Tabor, J. J., Simpson, Z. B., Lavery, L. A., Levy, M., Davidson, E. A., Scouras, A., Ellington, A. D., Marcotte, E. M., and Voigt, C. A. (2005) Synthetic biology: Engineering *Escherichia coli* to see light. *Nature 438*, 441−442.

(18) Möglich, A., and Moffat, K. (2007) Structural basis for light-dependent signaling in the dimeric LOV domain of the photosensor YtvA. *J. Mol. Biol. 373*, 112−126.

(19) Tabor, J. J., Levskaya, A., and Voigt, C. A. (2011) Multichromatic control of gene expression in *Escherichia coli*. *J. Mol. Biol. 405*, 315−324.

(20) Ryu, M. H., and Gomelsky, M. (2014) Near-infrared light responsive synthetic c-di-GMP module for optogenetic applications. *ACS Synth. Biol.*, DOI: 10.1021/sb400182x.

(21) Abe, K., Miyake, K., Nakamura, M., Kojima, K., Ferri, S., Ikebukuro, K., and Sode, K. (2014) Engineering of a green-light

inducible gene expression system in *Synechocystis* sp. PCC6803. *Microb. Biotechnol. 7*, 177−183.
(22) Shimizu-Sato, S., Huq, E., Tepperman, J. M., and Quail, P. H. (2002) A light-switchable gene promoter system. *Nat. Biotechnol. 20*, 1041−1044.
(23) Kennedy, M. J., Hughes, R. M., Peteya, L. A., Schwartz, J. W., Ehlers, M. D., and Tucker, C. L. (2010) Rapid blue-light-mediated induction of protein interactions in living cells. *Nat. Methods 7*, 973−975.
(24) Milias-Argeitis, A., Summers, S., Stewart-Ornstein, J., Zuleta, I., Pincus, D., El-Samad, H., Khammash, M., and Lygeros, J. (2011) *In silico* feedback for *in vivo* regulation of a gene expression circuit. *Nat. Biotechnol. 29*, 1114−1116.
(25) Yazawa, M., Sadaghiani, A. M., Hsueh, B., and Dolmetsch, R. E. (2009) Induction of protein-protein interactions in live cells using light. *Nat. Biotechnol. 27*, 941−945.
(26) Ye, H., Daoud-El Baba, M., Peng, R. W., and Fussenegger, M. (2011) A synthetic optogenetic transcription device enhances blood-glucose homeostasis in mice. *Science 332*, 1565−1568.
(27) Polstein, L. R., and Gersbach, C. A. (2012) Light-inducible spatiotemporal control of gene activation by customizable zinc finger transcription factors. *J. Am. Chem. Soc. 134*, 16480−16483.
(28) Müller, K., Engesser, R., Metzger, S., Schulz, S., Kämpf, M. M., Busacker, M., Steinberg, T., Tomakidi, P., Ehrbar, M., Nagy, F., Timmer, J., Zubriggen, M. D., and Weber, W. (2013) A red/far-red light-responsive bi-stable toggle switch to control gene expression in mammalian cells. *Nucleic Acids Res. 41*, e77.
(29) Müller, K., Engesser, R., Schulz, S., Steinberg, T., Tomakidi, P., Weber, C. C., Ulm, R., Timmer, J., Zurbriggen, M. D., and Weber, W. (2013) Multi-chromatic control of mammalian gene expression and signaling. *Nucleic Acids Res. 41*, e124.
(30) Crefcoeur, R. P., Yin, R., Ulm, R., and Halazonetis, T. D. (2013) Ultraviolet-B-mediated induction of protein−protein interactions in mammalian cells. *Nat. Commun. 4*, 1779.
(31) Cao, J., Arha, M., Sudrik, C., Bugaj, L. J., Schaffer, D. V., and Kane, R. S. (2013) Light-inducible activation of target mRNA translation in mammalian cells. *Chem. Commun. (Camb). 49*, 8338−8340.
(32) Motta-Mena, L. B., Reade, A., Mallory, M. J., Glantz, S., Weiner, O. D., Lynch, K. W., and Gardner, K. H. (2014) An optogenetic gene expression system with rapid activation and deactivation kinetics. *Nat. Chem. Biol. 10*, 196−202.
(33) Liu, H., Gomez, G., Lin, S., Lin, S., and Lin, C. (2012) Optogenetic control of transcription in zebrafish. *PLoS One 7*, e50738.
(34) Wang, X., Chen, X., and Yang, Y. (2012) Spatiotemporal control of gene expression by a light-switchable transgene system. *Nat. Methods 9*, 266−269.
(35) Konermann, S., Brigham, M. D., Trevino, A. E., Hsu, P. D., Heidenreich, M., Cong, L., Platt, R. J., Scott, D. A., Church, G. M., and Zhang, F. (2013) Optical control of mammalian endogenous transcription and epigenetic states. *Nature 500*, 472−476.
(36) Pathak, G. P., Vrana, J. D., and Tucker, C. L. (2013) Optogenetic control of cell function using engineered photoreceptors. *Biol. Cell. 105*, 59−72.
(37) Toettcher, J. E., Voigt, C. A., Weiner, O. D., and Lim, W. A. (2011) The promise of optogenetics in cell biology: Interrogating molecular circuits in space and time. *Nat. Methods 8*, 35−38.
(38) Gautier, A., Gauron, C., Volovitch, M., Bensimon, D., Jullien, L., and Vriz, S. (2014) How to control proteins with light in living systems. *Nat. Chem. Biol. 10*, 533−541.
(39) Gambetta, G. A., and Lagarias, J. C. (2001) Genetic engineering of phytochrome biosynthesis in bacteria. *Proc. Natl. Acad. Sci. U.S.A. 98*, 10566−10571.
(40) Olson, E. J., Hartsough, L. A., Landry, B. P., Shroff, R., and Tabor, J. J. (2014) Characterizing bacterial gene circuit dynamics with optically programmed gene expression signals. *Nat. Methods 11*, 449−455.
(41) Utsumi, R., Brissette, R. E., Rampersaud, A., Forst, S. A., Oosawa, K., and Inouye, M. (1989) Activation of bacterial porin gene expression by a chimeric signal transducer in response to aspartate. *Science 245*, 1246−1249.
(42) Hirose, Y., Shimada, T., Narikawa, R., Katayama, M., and Ikeuchi, M. (2008) Cyanobacteriochrome CcaS is the green light receptor that induces the expression of phycobilisome linker protein. *Proc. Natl. Acad. Sci. U.S.A. 105*, 9528−9533.
(43) Hirose, Y., Narikawa, R., Katayama, M., and Ikeuchi, M. (2010) Cyanobacteriochrome CcaS regulates phycoerythrin accumulation in *Nostoc punctiforme*, a group II chromatic adapter. *Proc. Natl. Acad. Sci. U.S.A. 107*, 8854−8859.
(44) Tabor, J. J., Salis, H. M., Simpson, Z. B., Chevalier, A. A., Levskaya, A., Marcotte, E. M., Voigt, C. A., and Ellington, A. D. (2009) A synthetic genetic edge detection program. *Cell 137*, 1272−1281.
(45) Davidson, E. A., Basu, A. S., and Bayer, T. S. (2013) Programming microbes using pulse width modulation of optical signals. *J. Mol. Biol. 425*, 4161−4166.
(46) Chan, L. Y., Kosuri, S., and Endy, D. (2005) Refactoring bacteriophage T7. *Mol. Syst. Biol. 1*, 2005.0018.
(47) Temme, K., Zhao, D., and Voigt, C. A. (2012) Refactoring the nitrogen fixation gene cluster from *Klebsiella oxytoca*. *Proc. Natl. Acad. Sci. U.S.A. 109*, 7085−7090.
(48) Anderson, J. C. (2006) Registry of Standard Biological Parts. Part: BBa_J23106. http://parts.igem.org/Part:BBa_J23106 (accessed, January 6, 2014).
(49) Salis, H. M., Mirsky, E. A., and Voigt, C. A. (2009) Automated design of synthetic ribosome binding sites to control protein expression. *Nat. Biotechnol. 27*, 946−950.
(50) Salis, H. M. (2011) The ribosome binding site calculator. *Methods Enzymol. 498*, 19−42.
(51) Ames, S. K., Frankema, N., and Kenney, L. J. (1999) C-terminal DNA binding stimulates N-terminal phosphorylation of the outer membrane protein regulator OmpR from *Escherichia coli*. *Proc. Natl. Acad. Sci. U.S.A. 96*, 11792−11797.
(52) Ninfa, A. J., Ninfa, E. G., Lupas, A. N., Stock, A., Magasanik, B., and Stock, J. (1988) Crosstalk between bacterial chemotaxis signal transduction proteins and regulators of transcription of the Ntr regulon: Evidence that nitrogen assimilation and chemotaxis are controlled by a common phosphotransfer mechanism. *Proc. Natl. Acad. Sci. U.S.A. 85*, 5492−5496.
(53) Groban, E. S., Clarke, E. J., Salis, H. M., Miller, S. M., and Voigt, C. A. (2009) Kinetic buffering of cross talk between bacterial two-component sensors. *J. Mol. Biol. 390*, 380−393.
(54) Yamamoto, K., Hirao, K., Oshima, T., Aiba, H., Utsumi, R., and Ishihama, A. (2005) Functional characterization *in vitro* of all two-component signal transduction systems from *Escherichia coli*. *J. Biol. Chem. 280*, 1448−1456.
(55) Comeau, D. E., Ikenaka, K., Tsung, K. L., and Inouye, M. (1985) Primary characterization of the protein products of the *Escherichia coli ompB* locus: Structure and regulation of synthesis of the OmpR and EnvZ proteins. *J. Bacteriol. 164*, 578−584.
(56) Huang, L., Tsui, P., and Freundlich, M. (1992) Positive and negative control of *ompB* transcription in *Escherichia coli* by cyclic AMP and the cyclic AMP receptor protein. *J. Bacteriol. 174*, 664−670.
(57) Zhou, L., Lei, X. H., Bochner, B. R., and Wanner, B. L. (2003) Phenotype microarray analysis of *Escherichia coli* K-12 mutants with deletions of all two-component systems. *J. Bacteriol. 185*, 4956−4972.
(58) Qi, L. S., Larson, M. H., Gilbert, L. A., Doudna, J. A., Weissman, J. S., Arkin, A. P., and Lim, W. A. (2013) Repurposing CRISPR as an RNA-guided platform for sequence-specific control of gene expression. *Cell 152*, 1173−1183.
(59) Yokobayashi, Y., Weiss, R., and Arnold, F. H. (2002) Directed evolution of a genetic circuit. *Proc. Natl. Acad. Sci. U.S.A. 99*, 16587−16591.
(60) Skerker, J. M., Perchuk, B. S., Siryaporn, A., Lubin, E. A., Ashenberg, O., Goulian, M., and Laub, M. T. (2008) Rewiring the specificity of two-component signal transduction systems. *Cell 133*, 1043−1054.
(61) Salis, H., Tamsir, A., and Voigt, C. (2009) Engineering bacterial signals and sensors. *Contrib. Microbiol. 16*, 194−225.

(62) Tabor, J. J., Groban, E. S., and Voigt, C. A. (2009) Performance characteristics for sensors and circuits used to program *E. coli*. In *Systems Biology and Biotechnology of Escherichia coli* (Lee, S. Y., Ed.), pp 401−439, Springer: Netherlands, Dordrecht.
(63) Ninfa, A. J. (2010) Use of two-component signal transduction systems in the construction of synthetic genetic networks. *Curr. Opin. Microbiol. 13*, 240−245.
(64) Whitaker, W. R., Davis, S. A., Arkin, A. P., and Dueber, J. E. (2012) Engineering robust control of two-component system phosphotransfer using modular scaffolds. *Proc. Natl. Acad. Sci. U.S.A. 109*, 18090−18095.
(65) Ganesh, I., Ravikumar, S., Lee, S. H., Park, S. J., and Hong, S. H. (2013) Engineered fumarate sensing *Escherichia coli* based on novel chimeric two-component system. *J. Biotechnol. 168*, 560−566.
(66) Cheng, R. R., Morcos, F., Levine, H., and Onuchic, J. N. (2014) Toward rationally redesigning bacterial two-component signaling systems using coevolutionary information. *Proc. Natl. Acad. Sci. U.S.A. 111*, E563−E571.
(67) Kopf, M., Klähn, S., Scholz, I., Matthiessen, J. K., Hess, W. R., and Voß, B. (2014) Comparative Analysis of the primary transcriptome of *Synechocystis* sp. PCC 6803. *DNA Res.*, DOI: 10.1093/dnares/dsu018.
(68) Solovyev, V., and Salamov, A. (2011) Automatic annotation of microbial genomes and metagenomic sequences. In *Metagenomics and Its Applications in Agriculture, Biomedicine, and Environmental Studies* (Li, R. W., Ed.), pp 61−78, Nova Science Publishers, New York.
(69) Batchelor, E., and Goulian, M. (2003) Robustness and the cycle of phosphorylation and dephosphorylation in a two-component regulatory system. *Proc. Natl. Acad. Sci. U.S.A. 100*, 691−696.
(70) Gao, R., and Stock, A. M. (2013) Probing kinase and phosphatase activities of two-component systems *in vivo* with concentration-dependent phosphorylation profiling. *Proc. Natl. Acad. Sci. U.S.A. 110*, 672−677.
(71) Chang, Y. C., Armitage, J. P., Papachristodoulou, A., and Wadhams, G. H. (2013) A single phosphatase can convert a robust step response into a graded, tunable, or adaptive response. *Microbiology 159*, 1276−1285.
(72) Menon, S., and Wang, S. (2011) Structure of the response regulator PhoP from *Mycobacterium tuberculosis* reveals a dimer through the receiver domain. *Biochemistry 50*, 5948−5957.
(73) Gao, R., and Stock, A. M. (2009) Biological insights from structures of two-component proteins. *Annu. Rev. Microbiol. 63*, 133−154.
(74) Barakat, M., Ortet, P., and Whitworth, D. E. (2011) P2CS: A database of prokaryotic two-component systems. *Nucleic Acids Res. 39*, D771−D776.
(75) Tabor, J. J., and Ellington, A. D. (2003) Playing to win at DNA computation. *Nat. Biotechnol. 21*, 1013−1015.
(76) Tabor, J. J. (2012) Modular gene-circuit design takes two steps forward. *Nat. Methods 9*, 1061−1063.
(77) Kotula, J. W., Kerns, S. J., Shaket, L. A., Siraj, L., Collins, J. J., Way, J. C., and Silver, P. A. (2014) Programmable bacteria detect and record an environmental signal in the mammalian gut. *Proc. Natl. Acad. Sci. U.S.A. 111*, 4838−4843.
(78) Sambrook, J., Fritsch, E. F., and Maniatis, T. (1989) *Molecular Cloning: A Laboratory Manual*, 2nd ed., Cold Spring Harbor Laboratory, Cold Spring Harbor, NY.
(79) Engler, C., Kandzia, R., and Marillonnet, S. (2008) A one pot, one step, precision cloning method with high throughput capability. *PLoS One 3*, e3647.